Communications in Computational Chemistry
Commun. Comput. Chem., Vol. 7, No. 4, 274–280
doi: 10.4208/cicc.2025.146.02
Regular Article

Benchmarking Density Functional Theory for Noble Metal Hydrides: A High-Fidelity PES and Vibrational Analysis of the $AgAuH^-$ Anion

Yuquan Feng[1], Kaiyi Zhao[1] and Jun Chen[1,2,*]

[1] *State Key Laboratory of Structural Chemistry, Fujian Institute of Research on the Structure of Matter, Chinese Academy of Sciences, Fuzhou 350002, China;*

[2] *Fujian Provincial Key Laboratory of Theoretical and Computational Chemistry, Xiamen 361005, China.*

[*] Corresponding author: chenjun@fjirsm.ac.cn

Received on 28 May 2025; Accepted on 9 June 2025

Abstract: The accurate description of noble metal hydrides remains a fundamental challenge for electronic structure theory, especially in systems involving heavy elements where relativistic effects and electron correlation are significant. In this study, we present a high-accuracy potential energy surface (PES) for the $AgAuH^-$ anion, constructed from 3,595 UCCSD(T)-F12a energy points and fitted using a feedforward neural network with a root mean square error of 0.21 meV. The PES captures the entire configuration space, including linear and bent minima, transition-state-like structures, and dissociation pathways. Quantum vibrational bound states were computed using time-independent quantum dynamics, enabling detailed mode assignments. The high-fidelity PES and vibrational dataset were used to benchmark some widely employed density functional theory (DFT) methods, B3LYP, ωB97XD, XYG3, and XYGJ-OS. Among these, XYGJ-OS provided the best agreement with the reference data in terms of equilibrium geometries and vibrational frequencies. This study provides a robust benchmark for method development and validation in metal-containing systems and highlights the importance of using high-level reference data when modeling complex coinage-metal hydrides.

Key words: $AgAuH^-$, density functional theory benchmarking, high-level *ab initio* potential energy surface, vibrational quantum dynamics, coinage metal hydrides.

1. Introduction

Gold and silver cluster compounds are key systems in catalysis, hydrogen storage, and photochemistry [1-4]. Due to their complex electronic structures and significant relativistic effects, accurate theoretical characterization remains challenging [5]. While density functional theory (DFT) is widely used due to its computational efficiency, most studies rely on low-rung functionals and static structures, leaving uncertainties regarding the predictive power of different methods [6]. In particular, the performance of DFT for systems containing coinage metals is highly functional-dependent, and systematic benchmark studies against high-level *ab initio* data are rarely reported [7-9].

Theoretically, the $AgAuH^-$ anion presents an ideal prototype to probe fundamental bonding, relativistic effects, and the reliability of electronic structure methods [10]. Its simplicity as a three-atom system allows for high-level quantum chemical treatment while still encapsulating the essential features of noble metal bonding. In addition, experimental

photoelectron spectra of AgAuH are feasible, but accurate vibrational assignments and spectroscopic interpretation remain incomplete, primarily due to the absence of reliable theoretical reference data.

A critical limitation in the field is the lack of benchmark datasets that combine high-fidelity potential energy surfaces (PESs) with corresponding vibrational state data. Such datasets are essential for testing and calibrating DFT and other computational methods. Given the increasing role of machine-learned PESs in molecular dynamics, having robust *ab initio*-based datasets is also indispensable for training and validating surrogate models [11,12].

In this study, we construct a high-accuracy PES for the $AgAuH^-$ anion based on CCSD(T)-F12a/aug-cc-pVTZ level of theory [13] and fitted using a feedforward neural network [14,15]. The resulting surface allows for precise vibrational state calculations using time-independent quantum dynamics. The computed dataset serves as a benchmark to systematically evaluate the performance of widely used DFT functionals, including B3LYP [16-18], ωB97XD [19], XYG3 [20], and XYGJ-OS [21], regarding structural, energetic, and vibrational predictions, providing a valuable reference for future spectroscopic and dynamical investigations.

The organization of this paper is delineated as follows: Section 2 provides an overview of theoretical methods, including PES construction and vibrational bound state calculations. In Section 3, a comparative analysis of the PES and vibrational states is conducted alongside the comparisons between density functional approximations and the CCSD(T) method, and discussions are made on the accuracy and availability of density functional approximations in the construction of high-level PESs. Finally, we conclude the paper in Section 4.

2. Theoretical method

2.1 Electronic structure calculations

All reference energy points were computed using the CCSD(T)-F12a method [13] with the aug-cc-pVTZ (augmented correlation-consistent polarized valence triple-zeta) basis set [22] for H and the aug-cc-pVTZ-PP (with pseudopotential) basis set [23] for Ag and Au. All coupled cluster calculations were performed using the MOLPRO 2020.1 software [24]. The dataset consists of 3,595 symmetry-unique geometries distributed over a broad configuration space, including both near-equilibrium and highly distorted geometries. These points were selected to uniformly sample the relevant bond lengths and angles to ensure global PES coverage.

In addition to the CCSD(T)-F12a calculations, two commonly used DFT methods, B3LYP [16-18], ωB97XD [19], as well as a series of xDH-type doubly hybrid functionals such as XYG3 [20] and XYGJ-OS [21], were also employed for comparison. Optimized geometries, harmonic frequencies, and single-point energies were obtained using these functionals with the same basis sets and pseudopotentials, ensuring consistency with the reference calculations. All DFT calculations were completed using a modified version of the Gaussian 16 program [25].

2.2 Neural network potential energy surface

A feedforward neural network (NN) model with architecture 3-30-30-1 was used to fit the PES [14,15,26]. Since the AgAuH system consists of three distinct atomic elements, permutation invariance among identical atoms is not a consideration. Therefore, the three internuclear distances (Ag-Au, Ag-H, and Au-H) were used directly as input features for the NN function. The network was trained using 90% from the CCSD(T)-F12a data set, with the remaining 10% reserved for validation. The final NN PES achieved a root mean square error (RMSE) of 0.21 meV, indicating excellent agreement with the high-level reference data throughout the full-dimensional configuration space. Details of the NN PES constructions can be found in our previously reported works [14,15,26-29].

2.3 Vibrational state calculations

Vibrational bound states were computed using a time-independent quantum dynamics approach. The nuclear Schrodinger equation was solved using discrete variable representation (DVR) in Jacobi coordinates (as illustrated in Figure 3). Specifically, a dense sampling of 199 points was used for the $R_{\text{Ag-Au}}$ distance, covering the range from 4.2 to 7.5 bohr, and likewise, 199 points were allocated for the $R_{\text{H-COM}}$ coordinate, extending from 0.0 to 9.5 bohr. The Jacobi angle θ was described using 30 distinct points. Nearly 50 bound states were determined using the Lanczos algorithm [30], spanning both the $[H\text{-}Ag\text{-}Au]^-$ and $[Ag\text{-}Au\text{-}H]^-$ isomers. Quantum numbers (v1, v2, v3) were assigned based on mode character and nodal patterns.

2.4 DFT benchmarking

DFT performance was evaluated by comparing optimized geometries, vibrational frequencies, and selected vibrational energy levels to the benchmark CCSD(T)-F12a results. Special attention was given to the Ag-Au stretching mode and the H-bending mode, which were found to be most sensitive to the choice of the functionals. Deviation metrics including mean absolute error (MAE) and root-mean-square deviation (RMSD) were computed to quantify the agreement.

3. Results and discussion

3.1 The CCSD(T)-F12a reference dataset

3.1.1 Stationary geometries and potential energy surface

Figure 1 summarizes the key stationary points located on the CCSD(T)-F12a/aug-cc-pVTZ potential energy surface of the $AgAuH^-$ anion. The figure includes both linear and bent structures, representing local minima and transition-state-like configurations. Bond lengths are given in Å, bond angles in degrees, and relative energies in red (in eV), with respect to the global minimum. These structures provide insight into the topography of the PES relevant to vibrational and isomerization dynamics.

The linear $[H\text{-}Ag\text{-}Au]^-$ geometry is confirmed as the global minimum, while a higher-energy local minimum corresponding to the $[Ag\text{-}Au\text{-}H]^-$ isomer is also identified. Two bent structures serve as transition states connecting these minima and exhibit distinct bonding characteristics.

In transition State 1, the H-Ag bond is short (1.596 Å), whereas the Ag-Au bond is longer (2.772 Å), indicating that the hydrogen atom is more strongly bonded to Ag, while Au is partially dissociated. Conversely, in transition State 2, the Au-H bond becomes dominant (1.563 Å) and the Ag-Au bond shortens to 2.660

Å, reflecting a shift of hydrogen binding preference toward Au. The bond angle increases from 58.61° in TS1 to 71.36° in TS2, indicating a more open configuration.

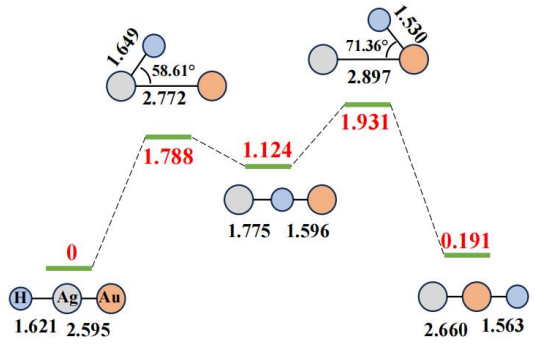

Figure 1. Stationary geometries and transition states of the $AgAuH^-$ anion on the CCSD(T)-F12a/aug-cc-pVTZ potential energy surface. Red numbers indicate relative energies (in eV) with respect to the global minimum. Bond lengths are given in Å and bond angles in degrees.

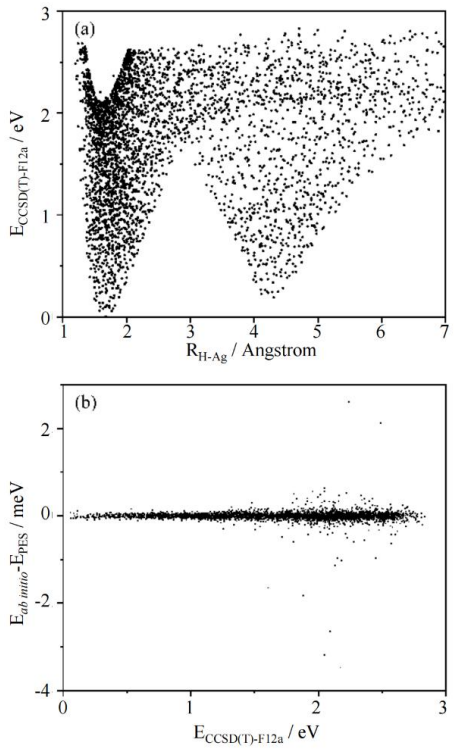

Figure 2. Overview of the CCSD(T)-F12a dataset and neural network PES fitting. (a) the distribution of all *ab initio* energy points in terms of the H-Ag bond length and total energy, covering a range of approximately 2.75 eV above the global minimum; (b) the fitting error of the PES relative to the CCSD(T)-F12a reference data.

This shift in hydrogen coordination from Ag to Au suggests a smooth but asymmetric isomerization pathway, governed by subtle electronic redistribution between the metal centers. The stronger H-Ag interaction in TS1 and the enhanced H-Au bonding in TS2 reflect the interplay of relativistic effects and d-orbital participation, which are essential features for accurate theoretical description. These observations further highlight the importance of a globally consistent PES that captures both near-linear and highly bent geometries for reliable modeling of metal-hydride systems.

To ensure reliable modeling of the $AgAuH^-$ anion across its full configuration space, we performed high-level *ab initio* calculations on a total of 3,595 symmetry-unique geometries using the CCSD(T)-F12a method. These points were carefully selected to span the relevant regions of the potential energy surface (PES), including equilibrium structures, bent intermediates, and dissociation channels, with energy values ranging up to approximately 2.75 eV above the global minimum.

Figure 2 provides an overview of the dataset and the performance of the neural network fitting. **Figure 2(a)** illustrates the distribution of data points in terms of the H-Ag bond length and total CCSD(T)-F12a energy. The sampling captures both short-range interactions and long-range dissociation behavior. **Figure 2(b)** shows the deviation between the NN predicted energy and the corresponding *ab initio* reference. Most of the fitting errors lie below 2 meV, confirming that the constructed PES accurately reproduces the energy landscape across diverse geometries. The overall fitting error (RMSE) is 0.21 meV. This level of fidelity ensures its suitability for subsequent quantum dynamics and functional benchmarking applications.

To further visualize the global structure of the potential energy surface, **Figure 3** presents a two-dimensional contour plot of the CCSD(T)-F12a PES in Jacobi coordinates. The horizontal axis represents the distance between the hydrogen atom and the center of mass of the Ag-Au dimer ($R_{H\text{-}COM}$), while the vertical axis corresponds to the angle θ formed by the three atoms. Notably, θ = 0° corresponds to the linear [Ag-Au-H]$^-$ geometry, and θ = 180° corresponds to the linear [H-Ag-Au]$^-$ configuration.

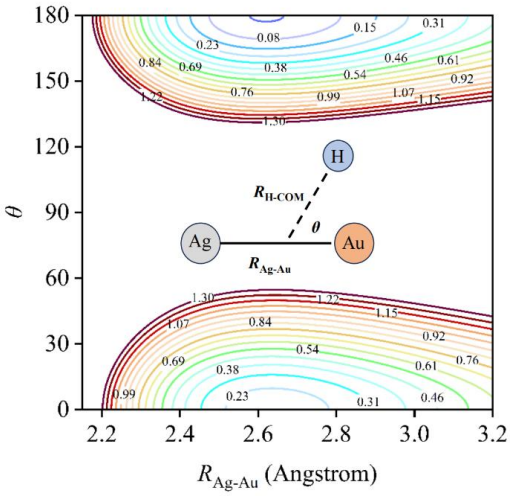

Figure 3. Two-dimensional contour plot of the CCSD(T)-F12a potential energy surface (PES) of $AgAuH^-$. The PES is plotted as a function of the Jacobi coordinates $R_{Ag\text{-}Au}$ and θ, where θ = 0° corresponds to the linear [Ag-Au-H]$^-$ geometry and θ = 180° corresponds to the [H-Ag-Au]$^-$ geometry. The plot illustrates a clear global minimum near θ = 180°, confirming that the linear [H-Ag-Au]$^-$ isomer is the most stable structure.

The plot clearly reveals that the global minimum of the PES lies near $\theta = 180^{\circ}$, confirming that the [H-Ag-Au]$^{-}$ geometry is the most stable arrangement. The symmetry and depth of the potential well around this minimum also support the vibrational analysis discussed later. The smoothness of the contour lines across both linear and bent regions further illustrates the robustness and transferability of the constructed PES across a broad configuration space.

3.1.2 Vibrational bound states

Table 1 summarizes the vibrational energy levels of the $AgAuH^{-}$ anion calculated on the potential energy surface of CCSD(T)-F12a. The states are labeled by their quantum numbers (ν_1, ν_2, ν_3), corresponding to excitations in the Ag-Au stretching, bending, and M-H stretching modes, respectively. The vibrational levels associated with the [Ag-Au-H]$^{-}$ isomer are marked with an asterisk(*), while all other states correspond to the [H-Ag-Au]$^{-}$ isomer.

The table lists nearly 50 bound vibrational levels with energies ranging from 1166 cm^{-1} to 3592 cm^{-1}, covering fundamental modes, overtones, and combination bands. The ground state of the [Ag-Au-H]$^{-}$ well appears as state 21, with its associated stretching and bending modes located at higher levels (e.g., states 27 and 49). This separation of vibrational ladders confirms the double-well nature of the PES and the significant energy barrier between the two isomers. The comprehensive level structure provides a benchmark for testing the accuracy of approximate quantum chemical methods and aids in the interpretation of experimental spectra.

Figure 4 displays the projected vibrational wavefunctions of selected bound states on the CCSD(T)-F12a PES, plotted as functions of the Ag-Au bond length ($R_{Ag\text{-}Au}$) and the Jacobi angle θ. These contour maps provide visual insight into the spatial distribution, nodal structure, and mode character of the vibrational eigenstates. These visualizations confirm the double-well character of the PES, illustrate the separation of isomer-specific vibrational ladders, and support the vibrational assignments listed in **Table 1**.

Table 1. Vibrational energy levels (in cm^{-1}) of the $HAgAu^{-}$ /$AgAuH^{-}$ anion calculated using the CCSD(T)-F12a PES. Levels marked with an asterisk (*) correspond to the [Ag-Au-H]$^{-}$ isomer, while the remaining levels correspond to the [H-Ag-Au]$^{-}$ isomer. Quantum numbers (ν_1, ν_2, ν_3) denote the Ag-Au stretching, bending, and M-H stretching modes, respectively.

State	E(cm^{-1})	Assignment	State	E(cm^{-1})	Assignment
1	1166	(0 0 0)	**26**	2966	(1 2 0)
2	1319	(1 0 0)	**27**	3013	(1 0 0)*
3	1470	(2 0 0)	**28**	3019	(2 0 1)
4	1621	(3 0 0)	**29**	3038	(8 1 0)
5	1770	(4 0 0)	**30**	3106	(13 0 0)
6	1850	(0 1 0)	**31**	3114	(2 2 0)
7	1918	(5 0 0)	**32**	3160	(2 0 0)*
8	2002	(1 1 0)	**33**	3170	(3 0 1)
9	2066	(6 0 0)	**34**	3186	(9 1 0)
10	2152	(2 1 0)	**35**	3255	(14 0 0)
11	2214	(7 0 0)	**36**	3261	(3 2 0)
12	2301	(3 1 0)	**37**	3306	(3 0 0)*
13	2362	(8 0 0)	**38**	3320	(4 0 1)
14	2449	(4 1 0)	**39**	3334	(10 1 0)
15	2510	(9 0 0)	**40**	3370	(0 3 0)
16	2597	(5 1 0)	**41**	3405	(15 0 0)
17	2659	(10 0 0)	**42**	3408	(4 2 0)
18	2666	(0 0 1)	**43**	3451	(4 0 0)*
19	2744	(6 1 0)	**44**	3469	(5 0 1)
20	2807	(11 0 0)	**45**	3482	(11 1 0)
21	2816	(0 0 0)*	**46**	3555	(1 1 1)
22	2865	(1 0 1)	**47**	3522	(5 2 0)
23	2867	(0 2 0)	**48**	3554	(16 0 0)
24	2891	(7 1 0)	**49**	3592	(0 1 0)*
25	2956	(12 0 0)			

Figure 4(a)–(c) correspond to low-energy vibrational states localized in the [H-Ag-Au]$^{-}$ well near $\theta = 180^{\circ}$, with minimal nodal features, representing the ground state and early excitations in the Ag-Au stretching coordinate. In contrast, Figure 4(d)-(f) show

wavefunctions centered near $\theta = 0^{\circ}$, associated with the [Ag-Au-H]$^{-}$ isomer. **Figure 4(d)** represents the vibrational ground state of this local minimum, while **Figure 4(e) and (f)** exhibit increasing nodal structure along the $R_{Ag\text{-}Au}$ coordinate, corresponding to the first and second Ag-Au stretching excitations. **Figure 4(i)** highlights a state with a prominent nodal structure along the θ coordinate, characteristic of a fundamental bending excitation. This state is more delocalized across angular space, consistent with the increased bending flexibility of the system compared to bond-stretching motions.

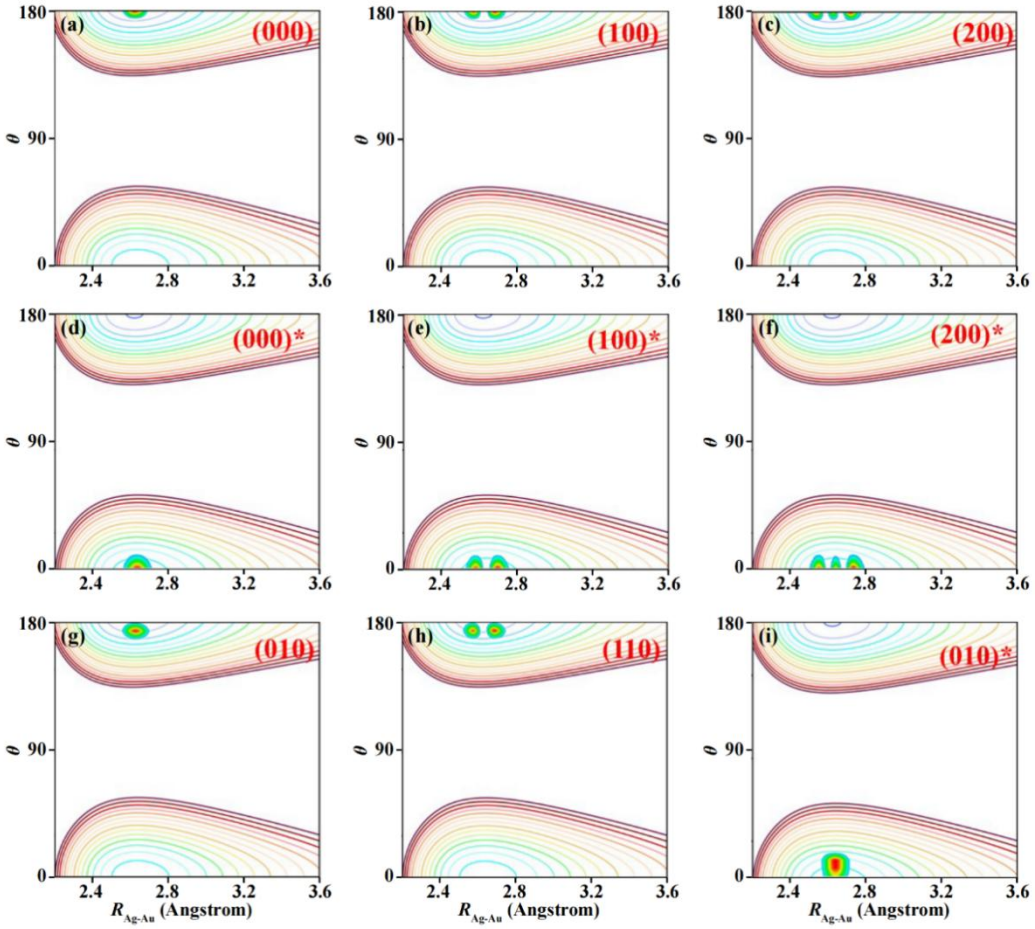

Figure 4. Projected vibrational wavefunctions of selected bound states of the AgAuH^{-} anion on the contour plot of the PES. Each panel shows the probability amplitude of a vibrational state as a function of the Ag-Au bond length ($R_{Ag\text{-}Au}$) and the Jacobi angle θ. The patterns illustrate nodal structure and localization of different modes, including Ag-Au stretching, bending, and M-H stretching contributions.

3.2 Benchmark of density functional approximations

3.2.1 Stationary geometries and potential energy surface

Table 2 presents the equilibrium bond lengths and vertical detachment energies (VDEs) of the [H-Ag-Au]$^{-}$ anion computed using a range of density functional methods, alongside the UCCSD(T)-F12a and UCCSD(T) reference values. The two widely used hybrid functionals, B3LYP and ωB97XD, produce significantly underestimated VDEs, by approximately 0.25 eV compared to the CCSD(T)-F12a benchmark, indicating their limited reliability in describing electron detachment in coinage-metal hydrides.

In contrast, xDH-type doubly hybrid functionals exhibit consistently improved performance. Most of them predict VDEs within 0.05 eV of the high-level reference, and their optimized geometries show better agreement with the CCSD(T) results. Notably, XYGJ-OS delivers the closest match in equilibrium bond lengths to the UCCSD(T)/aug-cc-pVTZ reference, indicating superior accuracy in structural prediction. When accounting for basis set completeness via the F12a approach, the differences between the xDH functionals become marginal, suggesting that several of these methods are robust choices for both structural and electronic property predictions in such systems.

3.2.2 Deviation of vibrational states

Beyond equilibrium structures and VDEs, we further constructed potential energy surfaces (PESs) for each of the tested methods based on their respective energy data, enabling non-harmonic vibrational frequency calculations. For each method, we identified and assigned the fundamental vibrational modes using the computed PES, including both isomer-specific states.

To systematically evaluate the accuracy of these functionals, we analyzed the deviations of their predicted vibrational energy levels relative to the CCSD(T)-F12a reference. Specifically, we focused on six key vibrational states: the ground state (000), the Ag-Au stretching fundamental (100), and the bending mode (010) of the [H-Ag-Au]$^{-}$ isomer, as well as their counterparts $(000)^{*}$, $(100)^{*}$, and $(010)^{*}$ in the [Ag-Au-H]$^{-}$ configuration.

As shown in **Figure 5**, the vibrational energy levels computed from PESs based on different methods exhibit varying degrees of

deviation from the CCSD(T)-F12a reference. xDH-type functionals generally yield smaller errors across all six representative modes, reflecting their improved ability to describe both electronic correlation and PES anharmonicity. In particular, the XYGJ-OS functional shows robust performance with errors typically below 50 cm^{-1}.

Table 2. Optimized equilibrium bond lengths (R_{H-Ag} and R_{Ag-Au}, in Å) and vertical detachment energies (VDE, in eV) of the [H-Ag-Au]$^-$ anion, computed using two representative hybrid functionals (B3LYP and ωB97XD) and a series of xDH-type doubly hybrid functionals. UCCSD(T) and UCCSD(T)-F12a values are provided for reference. All calculations were conducted at the basis set of aug-cc-pVTZ.

Method	R_{H-Ag}	R_{Ag-Au}	VDE / eV
UCCSD(T)-F12a	1.673	2.620	3.618
UCCSD(T)	1.659	2.633	3.572
B3LYP	1.662	2.674	3.350
ωB97XD	1.665	2.667	3.370
XYG3	1.655	2.624	3.525
XYG5	1.651	2.671	3.557
XYG6	1.653	2.616	3.625
XYG7	1.660	2.623	3.673
revXYG	1.652	2.613	3.605
XYGJ-OS	1.658	2.633	3.592

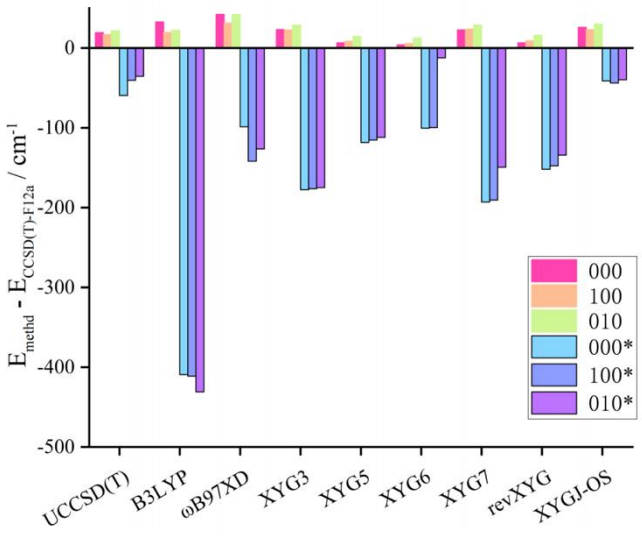

Figure 5. Deviation of vibrational energy levels (in cm^{-1}) calculated from different theoretical PESs relative to CCSD(T)-F12a reference values. Six representative states are included: (000), (100), (010) for the [H-Ag-Au]$^-$ isomer, and (000)* , (100)* , (010)* for the [Ag-Au-H]$^-$ isomer. The deviations from the CCSD(T)/aug-cc-pVTZ PES are also included for comparison.

In contrast, conventional hybrid functional B3LYP exhibits significantly larger deviations, even exceeding 400 cm^{-1}, indicating that conventional functionals may inadequately capture the curvature of the PES in soft vibrational coordinates.

4. Conclusion

In this work, we report a high-accuracy CCSD(T)-F12a potential energy surface (PES) for the $AgAuH^-$ anion, along with detailed vibrational eigenstate data obtained via quantum dynamics calculations. The PES spans a wide configurational space, including not only equilibrium structures but also transition-state-like geometries and dissociation regions, enabling rigorous treatment of anharmonicity and mode coupling. The resulting vibrational level structure, which includes both the [H-Ag-Au]$^-$ and [Ag-Au-H]$^-$ isomers, provides a benchmark for fundamental studies of vibrational spectroscopy and dynamics. This dataset can serve as a valuable reference for future investigations, including theoretical simulations of photoelectron spectra and vibrational state-resolved processes. All data, including structures, energies, and method-specific PESs, are openly available on GitHub [31].

Furthermore, we systematically evaluated the performance of several DFAs, with a particular focus on xDH-type doubly hybrid functionals. While traditional hybrid functionals such as B3LYP and ωB97XD exhibit notable errors in both geometry and vibrational frequency predictions, xDH functionals show consistently improved accuracy. Among them, XYGJ-OS delivers the best overall agreement with the CCSD(T)-F12a benchmarks across all evaluated properties, including bond lengths, vibrational energy levels, and vertical detachment energy. Given its computational scaling of only $O(N^4)$, XYGJ-OS stands out as a reliable and efficient choice for modeling coinage-metal hydrides and similar systems.

Acknowledgments

This work was financially supported by the National Natural Science Foundation of China (Grant No.22173104). We acknowledge FJOEL (Fujian Science & Technology Innovation Laboratory for Optoelectronic Information of China) for providing computation facilities.

References

[1] Xie H., Li X. Y., Zhao L. J., Liu Z. L., Qin Z. B., Wu X., Tang Z. C. and Xing X. P., Vibrationally resolved photoelectron imaging of Cu_2H^- and $AgCuH^-$ and theoretical calculations. *J. Phys. Chem. A*, **117** (2013), 1706–1711.

[2] Hong X., Yin Z. Y., Fan Z. X., Tay Y.-Y., Chen J. Z., Du Y. P., Xue C., Chen H. Y. and Zhang H., Periodic AuAg-Ag^2S heterostructured nanowires. *Small*, **2014**.

[3] Buckart S., Gantefoer G., Kim Y. D. and Jena P., Anomalous behavior of atomic hydrogen interacting with gold clusters. *J. Am. Chem. Soc.*, **125** (2003), 14205–14209.

[4] Hong X., Tan C. L., Liu J. Q., Yang J., Wu X.-J., Fan Z. X., Luo Z. M., Chen J. Z., Zhang X., Chen B. and Zhang H.,

AuAg nanosheets assembled from ultrathin AuAg nanowires. *J. Am. Chem. Soc.*, **137** (2015), 1444–1447.

[5] Xie H., Xing X. P., Liu Z. L., Cong R., Qin Z. B., Wu X., Tang Z. C. and Fan H. J., Photoelectron imaging and theoretical calculations of gold–silver hydrides: comparing the characteristics of Au, Ag and H in small clusters. *Phys. Chem. Chem. Phys.*, **14** (2012), 11666–11672.

[6] Ross R. B. and Ermler W. C., *Ab initio* calculations including relativistic effects for Ag_2, Au_2, AgAu, AgH, and AuH. *J. Phys. Chem.*, **89** (1985), 5202.

[7] Hodak J. H., Henglein A., Giersig M. and Hartland G. V., Laser-induced inter-diffusion in AuAg core-shell nanoparticles. *J. Phys. Chem. B*, **104** (2000), 11708–11718.

[8] Hodak J. H., Henglein A., Giersig M. and Hartland G. V., Synergistic effect in an Au-Ag alloy nanocatalyst: CO oxidation. *J. Phys. Chem. B*, **109** (2000), 40–43.

[9] Avramopoulos A., Ingamells V. E., Papadopoulos M. G. and Sadlej A. J., Vibrational corrections to electric properties of relativistic molecules: the coinage metal hydrides. *J. Phys. Chem. A*, **114** (2001), 198–210.

[10] Xie H., Xing X. P., Liu Z. L., Cong R., Qin Z. B., Wu X., Tang Z. C. and Fan H. J., Probing the structural and electronic properties of Ag_nH^- (n = 1–3) using photoelectron imaging and theoretical calculations. *J. Chem. Phys.*, **136** (2012), 184312.

[11] Zhao S., Liu Z.-P., Wang W.-Ni. and Nian F. K., Density functional study of small neutral and charged silver cluster hydrides. *J. Phys. Chem. A*, **110** (2006), 11537–11542.

[12] Kuang X. J., Wang X. Q. and Liu G. B., A density functional theory study on the Ag_nH (n = 1–10) clusters. *Struct. Chem.*, **22** (2011), 517–524.

[13] Knizia G., Adler T. B. and Werner H.-J., Simplified CCSD(T)-F12 methods: theory and benchmarks. *J. Chem. Phys.*, **130** (5) (2009).

[14] Chen J., Xu X., Xu X. and Zhang D. H., A global potential energy surface for the $H_2 + OH \leftrightarrow H_2O + H$ reaction using neural networks. *J. Chem. Phys.*, **138** (15) (2013), 154301.

[15] Chen J., Xu X., Xu X. and Zhang D. H., Communication: an accurate global potential energy surface for the $OH + CO \rightarrow H + CO_2$ reaction using neural networks. *J. Chem. Phys.*, **138** (22) (2013), 221104.

[16] Becke A. D., Density-functional exchange-energy approximation with correct asymptotic behavior. *Phys. Rev. A*, **38** (6) (1988), 3098.

[17] Lee C. T., Yang W. T. and Parr R. G., Development of the Colle-Salvetti correlation-energy formula into a functional of the electron density. *Phys. Rev. B*, **37** (2) (1988), 785.

[18] Stephens P. J., Devlin F. J., Chabalowski C. F. and Frisch M. J., *Ab initio* calculation of vibrational absorption and circular dichroism spectra using density functional force fields. *J. Phys. Chem.*, **98** (45) (1994), 11623–11627.

[19] Chai J.-D. and Gordon M. H., Long-range corrected hybrid density functionals with damped atom–atom dispersion corrections. *Phys. Chem. Chem. Phys.*, **10** (44) (2008), 6615–6620.

[20] Zhang Y., Xu X. and Goddard W. A., III., Doubly hybrid density functional for accurate descriptions of nonbond interactions, thermochemistry, and thermochemical kinetics. *Proc. Natl. Acad. Sci. USA*, **106** (13) (2009), 4963–4968.

[21] Zhang I. Y., Xu X., Jung Y. S. and Goddard W. A. III., A fast doubly hybrid density functional method close to chemical accuracy using a local opposite spin ansatz. *Proc. Natl. Acad. Sci. USA*, **108** (50) (2011), 19896–19900.

[22] Kendall R. A., Dunning T. H. Jr. and Harrison R. J., Electron affinities of the first-row atoms revisited: systematic basis sets and wave functions. *J. Chem. Phys.*, **96** (9) (1992), 6796–6806.

[23] Peterson K. A. and Puzzarini C., Systematically convergent basis sets for transition metals. II. pseudopotential-based correlation consistent basis sets for the group 11 (Cu, Ag, Au) and 12 (Zn, Cd, Hg) elements. *Theor. Chem. Acc.*, **114** (4–5) (2005), 283–296.

[24] Werner H.-J., Knowles P. J., Knizia G., Manby F. R., Schutz M., et al., Molpro, Version 2020.1, a Package of Ab Initio Programs. Molpro, 2012.

[25] Frisch M. J., et al., Gaussian 16, Revision C.01. Gaussian, Inc., Wallingford CT, 2016.

[26] Xu X., Chen J. and Zhang D. H., Global potential energy surface for the $H + CH_4 \leftrightarrow H_2 + CH_3$ reaction using neural networks. *Chin. J. Chem. Phys.*, **27** (4) (2014), 373–379.

[27] Chen J., Sun Z. G. and Zhang D. H., An accurate potential energy surface for the $F + H_2 \rightarrow HF + H$ reaction by the coupled-cluster method. *J. Chem. Phys.*, **142** (2) (2015), 024303.

[28] Chen J. and Zhang D. H., Construction of molecular reactive potential energy surfaces based on neural networks. *Sci. Sin. Chim.*, **45** (12) (2015), 1241–1253.

[29] Shen X. J., Chen J., Zhang Z. J., Shao K. J. and Zhang D. H., Methane dissociation on Ni(111): a fifteen-dimensional potential energy surface using neural network method. *J. Chem. Phys.*, **143** (14) (2015), 144701.

[30] Lanczos C., An iteration method for the solution of the eigenvalue problem of linear differential and integral operators. *J. Res. Natl. Bur. Stand.*, **45** (4) (1950), 255–282.

[31] The $AgAuH^-$ anion dataset. Github repository, 2025. Available at: https://github.com/njuchenjun/agauh_anion.